



Title	Direct Comparison Between Magnetospheric Plasma Waves and Polar Mesosphere Winter Echoes in Both Hemispheres
Authors	Y.M. Tanaka, T. Nishiyama, A. Kadokura, M. Ozaki, Y. Miyoshi, K. Shiokawa, S.I. Oyama ¹ , R. Kataoka, M. Tsutsumi, K. Nishimura, K. Sato, Y. Kasahara, A. Kumamoto, F. Tsuchiya, M. Fukizawa, M. Hikishima, S. Matsuda, A. Matsuoka, I. Shinohara, M. Nosé, T. Nagatsuma, M. Shinohara, A. Fujimoto, M. Teramoto, R. Nomura, A. Sessai Yukimatu, K. Hosokawa, M. Shoji, R. Latteck
Citation	Journal of Geophysical Research: Space Physics, 124, 9626-9639 , 2019
Issue Date	2019-11-26
Type	Journal Article
URL	https://doi.org/10.1029/2019JA026891
Right	
Textversion	publisher

JGR Space Physics

RESEARCH ARTICLE

10.1029/2019JA026891

Key Points:

- EMIC waves and chorus waves in the magnetosphere and PMWE in the mesosphere were observed simultaneously by the conjugate observation
- PMWE were detected by the PANSY and MAARSY radars in both Northern and Southern Hemispheres during the equinox period
- The temporal variation of the chorus wave power was quite similar to those of PMWE powers observed in both hemispheres

Supporting Information:

- Supporting Information S1
- Movie S1

Correspondence to:

Y.-M. Tanaka,
ytanaka@nipr.ac.jp

Citation:

Tanaka, Y.-M., Nishiyama, T., Kadokura, A., Ozaki, M., Miyoshi, Y., Shiokawa, K., et al. (2019). Direct comparison between magnetospheric plasma waves and polar mesosphere winter echoes in both hemispheres. *Journal of Geophysical Research: Space Physics*, 124, 9626–9639. <https://doi.org/10.1029/2019JA026891>






























Received 25 APR 2019

Accepted 2 SEP 2019

Accepted article online 10 OCT 2019

Published online 26 NOV 2019

Direct Comparison Between Magnetospheric Plasma Waves and Polar Mesosphere Winter Echoes in Both Hemispheres

Y.-M. Tanaka^{1,2,3} , T. Nishiyama^{1,3} , A. Kadokura^{1,2,3} , M. Ozaki⁴ , Y. Miyoshi⁵ , K. Shiokawa⁵ , S.-I. Oyama^{1,5,6} , R. Kataoka^{1,3} , M. Tsutsumi^{1,3} , K. Nishimura^{1,2,3} , K. Sato⁷ , Y. Kasahara⁴ , A. Kumamoto⁸ , F. Tsuchiya⁸ , M. Fukizawa⁸ , M. Hikishima⁹ , S. Matsuda⁹ , A. Matsuoka⁹ , I. Shinohara⁹ , M. Nosé⁵ , T. Nagatsuma¹⁰ , M. Shinohara¹¹ , A. Fujimoto¹² , M. Teramoto⁵ , R. Nomura¹³ , A. Sessai Yukimatu^{1,3} , K. Hosokawa¹⁴ , M. Shoji⁵ , and R. Latteck¹⁵ 

¹National Institute of Polar Research, Tokyo, Japan, ²Polar Environment Data Science Center, Joint Support-Center for Data Science Research, Research Organization of Information and Systems, Tokyo, Japan, ³Department of Polar Science, The Graduate University for Advanced Studies, SOKENDAI, Japan, ⁴Graduate School of Natural Science and Technology, Kanazawa University, Kanazawa, Japan, ⁵Department of Space Systems Engineering, Faculty of Engineering, Kyushu Institute of Technology, Kitakyushu, Japan, ⁶Ionosphere Research Unit, University of Oule, Oulu, Finland, ⁷Department of Earth and Planetary Science, The University of Tokyo, Tokyo, Japan, ⁸Graduate School of Science, Tohoku University, Sendai, Japan, ⁹Institute of Space and Astronautical Science, Japan Aerospace Exploration Agency, Tokyo, Japan, ¹⁰National Institute of Information and Communications Technology, Tokyo, Japan, ¹¹Department of Liberal Arts and Sciences, National Institute of Technology Kagoshima College, Kirishima, Japan, ¹²Department of Artificial Intelligence, Faculty of Computer Science and Systems Engineering, Kyushu Institute of Technology, Kitakyushu, Japan, ¹³National Astronomical Observatory of Japan, Tokyo, Japan, ¹⁴Graduate School of Informatics and Engineering, The University of Electro-Communications, Tokyo, Japan, ¹⁵Leibniz Institute of Atmospheric Physics, Kühlungsborn, Germany

Abstract We present the first and direct comparison between magnetospheric plasma waves and polar mesosphere winter echoes (PMWE) simultaneously observed by the conjugate observation with Arase satellite and high-power atmospheric radars in both hemispheres, namely, the Program of the Antarctic Syowa Mesosphere, Stratosphere, and Troposphere/Incoherent Scatter Radar at Syowa Station (SYO; -69.00°S , 39.58°E), Antarctica, and the Middle Atmosphere Alomar Radar System at Andøya (AND; 69.30°N , 16.04°E), Norway. The PMWE were observed during 03–07 UT on 21 March 2017, just after the arrival of corotating interaction region in front of high-speed solar wind stream. An isolated substorm occurred at 04 UT during this interval. Electromagnetic ion cyclotron (EMIC) waves and whistler mode chorus waves were simultaneously observed near the magnetic equator and showed similar temporal variations to that of the PMWE. These results indicate that chorus waves as well as EMIC waves are drivers of precipitation of energetic electrons, including relativistic electrons, which make PMWE detectable at 55- to 80-km altitude. Cosmic noise absorption measured with a 38.2-MHz imaging riometer and low-altitude echoes at 55–70 km measured with a medium-frequency radar at SYO also support the relativistic electron precipitation. We suggest a possible scenario in which the various phenomena observed in near-Earth space, such as magnetospheric plasma waves (EMIC waves and chorus waves), pulsating auroras, cosmic noise absorption, and PMWE, can be explained by the interaction between the high-speed solar wind containing corotating interaction regions and the magnetosphere.

1. Introduction

Energetic electron precipitation during geomagnetic disturbances plays a key role in coupling between near-Earth space and the polar atmosphere. The energetic electrons penetrate the upper atmosphere and deposit energy through ionization, dissociation, and excitation of atmospheric constituents. They cause auroral optical emissions in the ionospheric *E* region at an altitude of 90–150 km (corresponding to precipitation of electrons with energy *E* of several to several tens of kiloelectron volts), absorption of cosmic radio noise in the ionospheric *D* region at 60–90 km (*E* of several tens to several hundreds of kiloelectron volts), and backscatter radar echoes from the mesosphere at 50–80 km (*E* of several tens of kiloelectron volts to

several megaelectron volts; cf., Figure 4a in this paper; S. Kasahara, Miyoshi, et al., 2018; Miyoshi et al., 2010; Miyoshi, Saito, et al., 2015; Nishimura et al., 2010; Nishiyama et al., 2018; Tanaka et al., 2005). In particular, special attention has been paid to the precipitation of relativistic electrons with E greater than 500 keV because they reach an altitude lower than 70 km. There they increase concentrations of nitric oxides (NO_x) and hydrogen oxides (HO_x), which deplete the ozone layer in the stratosphere through catalytic cycles directly or indirectly after downward transport during the polar winter (Kirkwood, Osepian, Belova, Urban, et al., 2015; Shinnhuber et al., 2012; Thorne, 1977; Turunen et al., 2016).

The major candidate mechanism for relativistic electron precipitation (REP) is pitch angle scattering of trapped energetic electrons due to interaction with plasma waves in the magnetosphere. Such waves include electromagnetic ion cyclotron (EMIC) waves in a frequency range from 0.1 to 5 Hz and very low frequency (VLF) band waves with a frequency between several hundreds of hertz and 10 kHz, such as whistler mode chorus waves. EMIC waves have been identified as a potential driver of the precipitation of not only energetic ions with energy of tens of kiloelectron volts (e.g., Lyons & Thorne, 1972; Ozaki et al., 2016) but also relativistic electrons with energy of sub-megaelectron volts or greater than 1 MeV (Miyoshi et al., 2008; Ozaki, Shiokawa, Miyoshi, Kataoka, et al., 2018; Thorne & Kennel, 1971). EMIC waves excited in the equatorial magnetosphere propagate along the field line to the ionosphere and are observed as Pc 1 geomagnetic pulsations on the ground (Saito, 1969). Simultaneous observations of REP with EMIC waves and/or Pc 1 pulsations have been reported by some case studies (e.g., Miyoshi et al., 2008) and statistical studies (e.g., Hendry et al., 2017).

On the other hand, debate continues on whether chorus waves are responsible for REP because of a lack of observational evidence. It has been revealed that chorus waves can precipitate electrons with energy of several tens of kiloelectron volts that cause pulsating aurora as well as to a few hundreds of kiloelectron volts (S. Kasahara, Miyoshi, et al., 2018; Miyoshi et al., 2010; Miyoshi, Saito, et al., 2015; Nishimura et al., 2010; Ozaki, Shiokawa, Miyoshi, Hosokawa, et al., 2018). Miyoshi, Oyama, et al. (2015) demonstrated by observation with European Incoherent Scatter Tromsø very high frequency (VHF) radar that electron density increased at altitude as low as 68 km in association with pulsating aurora, and such a low-altitude ionization can be explained by the precipitation of energetic electrons with E up to at least 200 keV, which were precipitated by the interaction with lower band chorus (LBC) waves. Since chorus waves occur commonly in the magnetosphere over a wide range of longitudes from midnight to noon during substorms, the impact of chorus wave-driven REP on the deep atmosphere is significant (Turunen et al., 2016).

In order to investigate the drivers of REP, we compare magnetospheric plasma waves with polar mesosphere winter echoes (PMWE). PMWE are observed in the polar mesosphere between 50 and 80 km with VHF (30–300 MHz) radars during winter periods (from September to March in the Northern Hemisphere and from March to September in the Southern Hemisphere; Kirkwood, 2007; Latteck & Strelnikova, 2015; Nishiyama et al., 2015). They are often observed when electron density in the mesosphere is highly enhanced by energetic proton precipitation during solar proton events or energetic electron precipitation during substorms (Kirkwood et al., 2002; Nishiyama et al., 2018). PMWE are mainly detected in daytime and not in nighttime because of the reduction in electron density due to the recombination and the increase in electron diffusivity, which is caused by the attachment of electrons to form negative ions, in nighttime. Polar mesosphere summer echoes (PMSE), which are very strong radar backscatters from the polar mesosphere at 80–90 km during summer, have been studied by a large number of observational and theoretical studies since 1980s, and it is widely accepted that PMSE are caused by a combination of neutral turbulence and charged ice particles (see Rapp & Lübken, 2004). On the other hand, PMWE have been less noticed and still poorly understood because they are much weaker and therefore less frequently observed than PMSE.

PMWE are coherent Bragg scattering from the mesosphere. The Bragg condition requires fluctuations in refractive index, which is mainly given by the electron number density in the mesosphere, on the scale of half the radar wavelength (~ 3 m for VHF radars used in this study). The plausible mechanism creating such small-scale structures of electron density is neutral atmospheric turbulence, which is induced by wind shear or associated with breaking of atmospheric gravity waves (Balsley et al., 1983; Belova et al., 2005; Czechowsky et al., 1989; Lübken et al., 2006). Combined observation with in situ rocket and VHF radar demonstrated that some of PMWE events could be attributed to strong neutral turbulence and high electron density (Lübken et al., 2006). However, some radar observations showed that PMWE could not be reasonably explained by the turbulence only. Kirkwood et al. (2006) suggested that such PMWE are caused by scatter

from evanescent ion acoustic waves associated with reflection of infrasonic waves at wind shears or temperature inversions. Furthermore, due to analogy with PMSE, it has been discussed whether charged dust particles exist in the PMWE layers, although the temperature in the winter mesosphere is too high to form ice particles. Some artificial heating experiments clarified the overshoot effect on PMWE after heater turnoff, which indicates the presence of charged dust particles (Belova et al., 2008; La Hoz & Havnes, 2008).

We conducted simultaneous observations with the Arase satellite, which was launched in December 2016 (Miyoshi et al., 2018) and well-coordinated ground-based instruments in the Northern and Southern Hemispheres. The main period of interest is 02:00–07:00 UT on 21 March 2017, just after the arrival of corotating interaction region (CIR), during which Arase was in the equatorial magnetosphere on the morning side (cf., Figure 4b). If REP is due to plasma waves near the equatorial magnetosphere, it should affect both hemispheres. An advantage of this study is mesospheric observations with two high power VHF radars, namely, the Program of the Antarctic Syowa Mesosphere, Stratosphere, and Troposphere/Incoherent Scatter Radar (PANSY; Sato et al., 2014) in the Southern Hemisphere and the Middle Atmosphere Alomar Radar System (MAARSY; Latteck et al., 2012) in the northern hemisphere.

The PANSY radar is a mesosphere-stratosphere-troposphere radar installed at Syowa Station (SYO; -69.00°S , 39.58°E), Antarctica, with an operating frequency of 47 MHz and a large peak power (~ 520 kW). It consists of an active phased array of 1,045 Yagi antennas, which forms a large antenna aperture (about $180,000\text{ m}^2$). As of August 2019, the radar had been in full and continuous operation since late September 2015, using five beams, that is, local zenith, geographic north, east, south, and west with a zenith angle of 10° . The range resolution is 600 m, and the temporal resolution is about 4 min, including the observations in both the mesospheric and tropospheric-stratospheric modes. The MAARSY is also a mesosphere-stratosphere-troposphere radar at Andøya (AND; 69.30°N , 16.04°E), Norway. The system is composed of an active phased antenna consisting of 433 array elements and an identical number of transceiver modules. The operational radar frequency is 53.5 MHz, and the maximum peak power is approximately 800 kW. The 433 antennas arranged in an equilateral triangle grid structure form a nearly circular antenna array with an aperture of $\sim 6,300\text{ m}^2$ and a symmetric beam of 3.6° (full width at half power). During winter 2016/2017 MAARSY was operated in a combined tropospheric/mesospheric mode with a range resolution of 300 m and a temporal resolution of about 2.5 min for the experimental sequence.

2. Results

Magnetospheric plasma waves and PMWE were observed under the following ideal conditions. First, the Arase footprints were close to SYO, Antarctica, and Husafell (HUS; 65.67°N , -21.03°E), Iceland, which are a rare pair of geomagnetic conjugate stations. Figure 1 shows the Arase footprints at 100-km altitude in the Northern and Southern Hemispheres during the period 03:00 to 07:00 UT on 21 March, which were calculated with the Tsyganenko and Sitnov TS04 model (Tsyganenko & Sitnov, 2005). Second, various phenomena were sufficiently quiet before the arrival of the CIR to make the relationship between them clear. Figure 2 exhibits the relationship between solar wind speed, geomagnetic variation, and PMWE observed at SYO during the period from 17 to 31 March. The geomagnetic activity and PMWE power at 55–80 km were weak before the arrival of the high-speed solar streams (HSS) and increased after 21 March. Third, since it was the equinox, the PMWE observed only during winter were detected in both hemispheres.

Figure 3 shows solar wind and geomagnetic conditions during the period from 20 UT on 20 March to 16 UT on 21 March. During this period, the solar wind speed increased from 300 to 600 km/s (Figure 3a) and the CIR at the leading edges of HSS arrived. Typical CIR characteristics were observed, such as enhanced solar wind dynamic pressure (Figure 3d) and a highly fluctuating north-south component of the interplanetary magnetic field (Figure 3c) (Crooker & Cliver, 1994; Kataoka & Miyoshi, 2006; Richardson et al., 2006; Tsurutani et al., 1995). These solar wind disturbances gave rise to magnetospheric compression and an isolated substorm, which was identified by the enhancement in AE index (Figure 3e).

Figures 4c–4i show the relation between magnetospheric plasma waves and ionospheric and mesospheric phenomena in both hemispheres. An isolated substorm started at 04:00 UT, as indicated by the negative bay-shaped variation in the northward component of the magnetic field at SYO and Pi 2 pulsations in the band-pass filtered (40–150 s) magnetic field (Figure 4i). The negative bay magnetic variation was due to

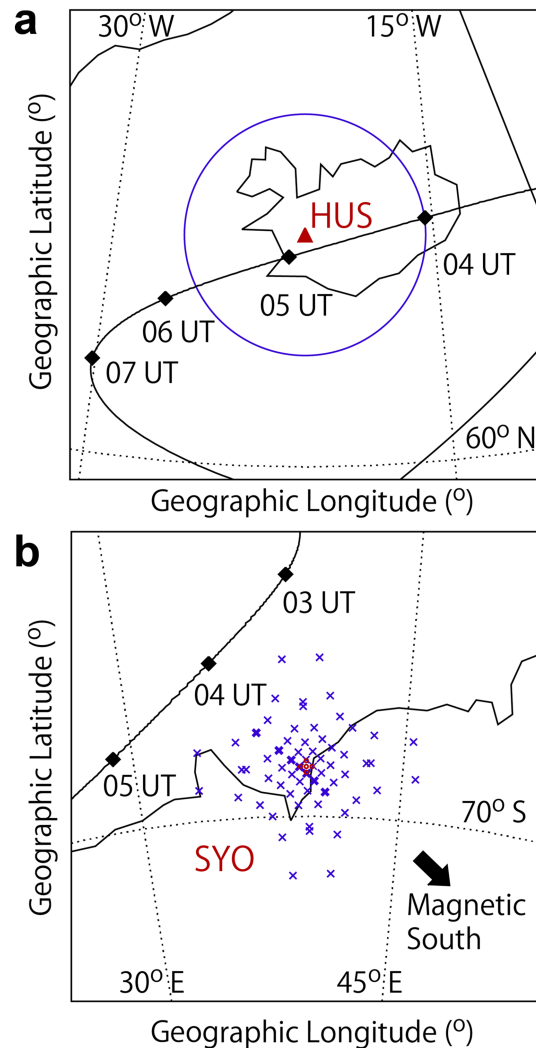


Figure 1. Arase footprints at 100 km over HUS, Iceland, and SYO, Antarctica, during the period from 03:00 to 07:00 UT on 21 March 2017, which were calculated using the Tsyganenko and Sitnov TS04 model. (a) The blue circle shows the field of view of the all-sky imager at HUS, calculated assuming a 70° zenith angle and 105-km altitude. (b) The small red circles around the center indicate the locations of the five Program of the Antarctic Syowa Mesosphere, Stratosphere, and Troposphere/Incoherent Scatter Radar beams at 70 km (local zenith, geographic north, east, south, and west with a zenith angle of 10°), and the blue crosses show the positions of the 8 × 8 beams of the 38.2-MHz imaging riometer at 90 km over SYO.

the westward auroral electrojet current in the ionosphere. Two types of plasma waves were detected in the magnetosphere: upper band chorus and LBC waves in the frequency range of 0.3–4.0 kHz during 04:45–07:00 UT (Figure 4e), corresponding to the recovery phase of the substorm, and intermittent EMIC waves at 0.2–0.5 Hz during 02:30–04:45 UT, including the interval before the substorm onset (Figure 4f). These waves were detected with the Onboard Frequency Analyzer of the Plasma Wave Experiment (Y. Kasahara, Kasaba, et al., 2018, Matsuda et al., 2018; Ozaki, Yagitani, Kasahara, Kojima, et al., 2018) and the Magnetic Field Experiment onboard Arase (Matsuoka et al., 2018), respectively. The local cyclotron frequency was derived from the Magnetic Field Experiment data. The rising tone elements of the chorus and EMIC waves were not observed during the period from 02:00 to 07:00 UT. As shown at the top of the figure, we define interval (A) as the time before substorm onset (02:00–04:00 UT), interval (B) as the time during which the enhancement of plasma waves was observed in the broad frequency range of ULF, ELF, and VLF just after the onset (04:00–04:45 UT), and interval (C) as the time during which chorus waves were observed (04:45–07:00 UT).

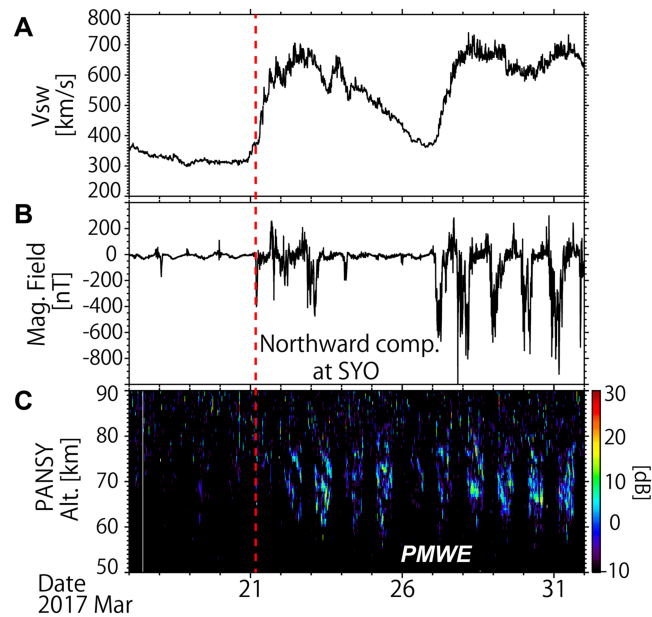


Figure 2. Relationship between solar wind speed, geomagnetic variation, and PMWE observed at SYO from 17 to 31 March. (a) Solar wind speed. (b) Northward component of the magnetic field at SYO. (c) Mesospheric echo power for the zenith beam of the Program of the Antarctic Syowa Mesosphere, Stratosphere, and Troposphere/Incoherent Scatter Radar. The red vertical dashed line indicates the beginning of an isolated substorm (at 04:00 UT on 21 March). PMWE = polar mesosphere winter echoes.

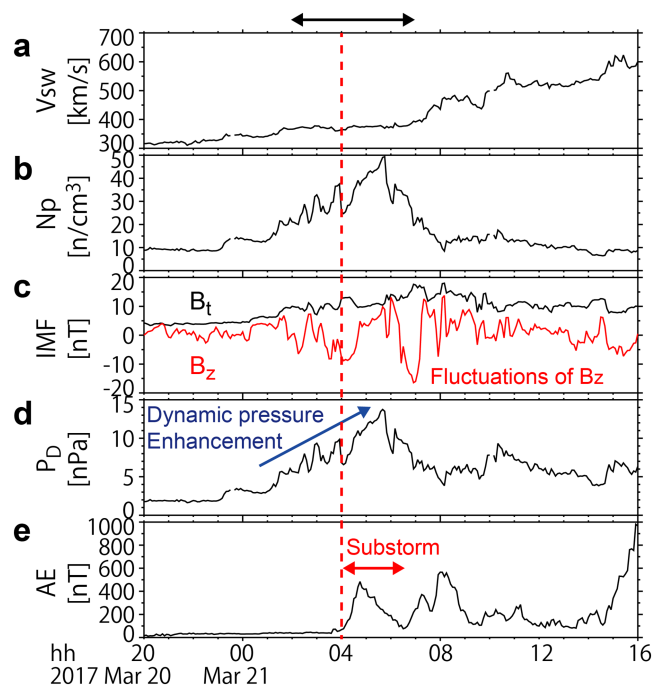


Figure 3. Solar wind parameters during the period from 20:00 UT on 20 March to 16:00 UT on 21 March 2017. The horizontal arrow at the top shows the period that is the focus of this study. (a) Solar wind speed. (b) Proton density. (c) Magnitude (B_t) and northward component (B_z) of the interplanetary magnetic field in the geocentric solar magnetospheric coordinate system. (d) Dynamic pressure. (e) AE index, which is an indicator of the auroral activity produced using geomagnetic field data from auroral latitudes. The solar wind data have been shifted in time to the bow shock nose.

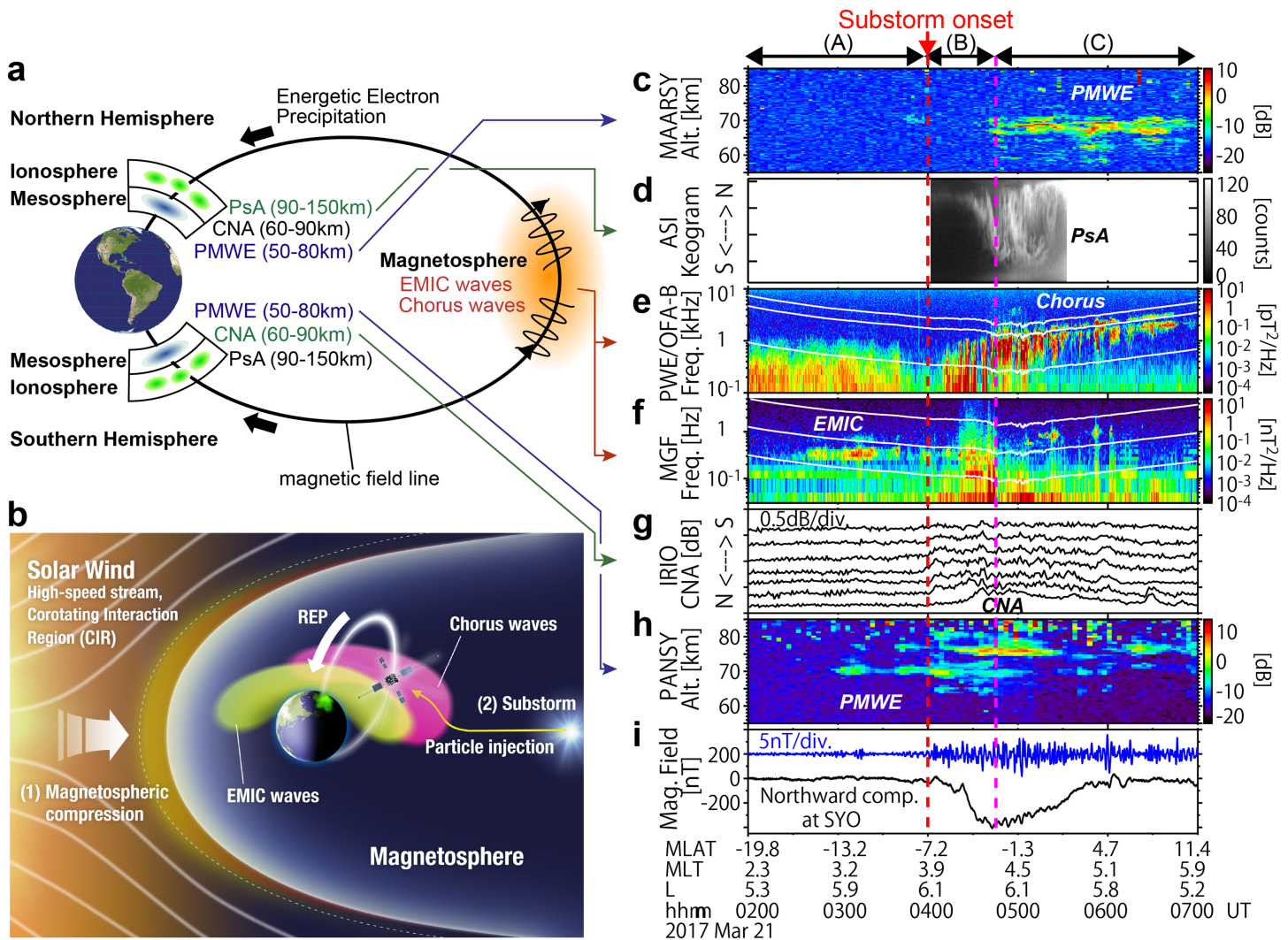


Figure 4. Coordinated observation in multiple regions during 02:00–07:00 UT on 21 March 2017. (a) Schematic of various phenomena observed in multiple regions during 02:00–07:00 UT on 21 March. Plasma waves (electromagnetic ion cyclotron [EMIC] waves and chorus waves) in the magnetosphere were observed by the Arase satellite. Pulsating auroras (PsA) in the ionospheric *E* region, cosmic noise absorption (CNA) in the ionospheric *D* region, and polar mesosphere winter echoes (PMWE) in the mesosphere were observed from the ground in both hemispheres. (b) Summary of phenomena observed in the solar wind and the magnetosphere. (c) Mesospheric echo power measured with the MAARSY radar at AND, Norway. (d) Auroral luminosity along the north-south magnetic meridian obtained with the all-sky imager (ASI) at HUS, Iceland. (e) Dynamic spectrum of the magnetic field observed with the Onboard Frequency Analyzer (OFA) of the Plasma Wave Experiment (PWE) onboard Arase. The location of Arase is shown under panel (i), where MLAT, MLT, and L mean magnetic latitude, magnetic local time, and L value, respectively. The white lines in panel (e) show $0.1f_{ce}$, $0.5f_{ce}$, and $0.8f_{ce}$ from the bottom, where f_{ce} is the electron cyclotron frequency. The magnitude of local magnetic field observed by Arase was used for the calculation. (f) Dynamic spectrum of the Z component of the magnetic field in the Despun Sun sector Inertia coordinate obtained by the Magnetic Field Experiment (MGF) onboard Arase. This component travels along the satellite spin axis and generally toward the Sun with a deviation of $1 \pm 5^\circ$. The white lines show the oxygen, helium, and proton cyclotron frequencies from the bottom. (g) Cosmic noise absorption (CNA) observed with the imaging riometer (IRIO) at SYO, Antarctica. (h) Mesospheric echo power measured with the PANSY radar at SYO. The result shown is the average of five beams. (i) Northward component of the magnetic field (black curve) at SYO and its data filtered in the time range of 40–150 s (blue curve). MAARSY = Middle Atmosphere Alomar Radar System; PANSY = Program of the Antarctic Syowa Mesosphere, Stratosphere, and Troposphere/Incoherent Scatter Radar.

In the Southern Hemisphere, an enhancement of cosmic noise absorption (CNA) in the ionosphere was observed with the imaging riometer at SYO just after the onset (Figure 4g), which indicates precipitation of electrons with *E* of several tens to several hundreds of kiloelectron volts (e.g., Tanaka et al., 2005 and their references). The imaging riometer at SYO measures two-dimensional distribution of CNA at a frequency of 38.2 MHz (Figure 1b). In Figure 4g, the CNA data from seven beams along the magnetic meridian, shown by thick crosses in Figure 1b, were plotted. The data from the southernmost beams were not analyzed in this study because the receiver for the beams was out of order. PMWE enhancement was simultaneously

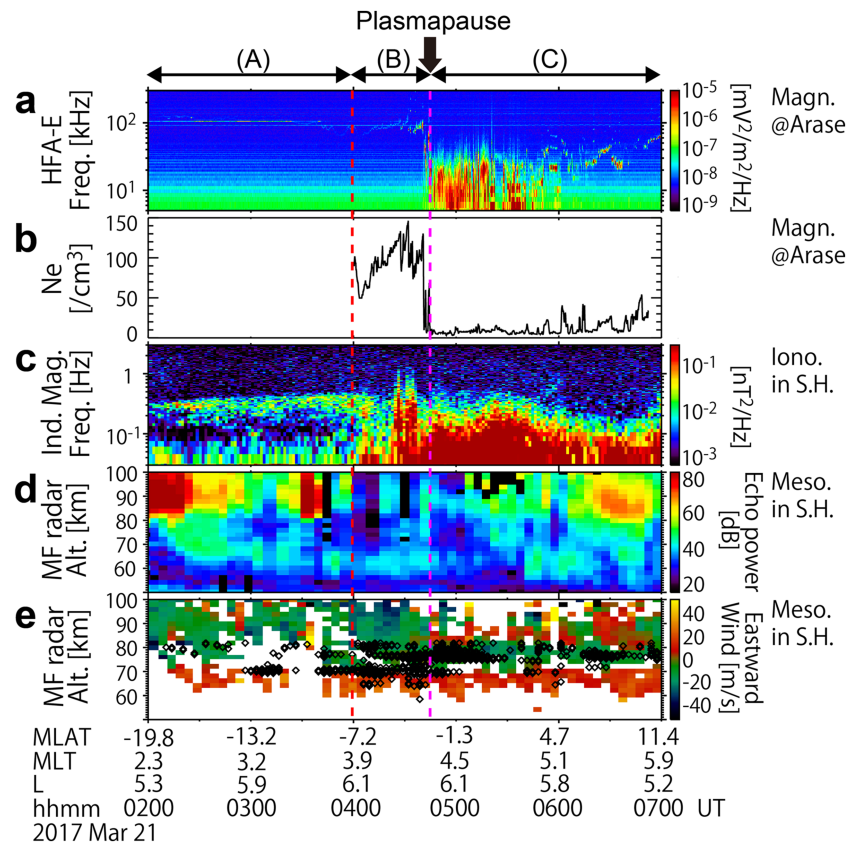


Figure 5. Supplementary data sets obtained by the Arase satellite and ground-based observations during 02:00–07:00 UT on 21 March. (a) Dynamic spectrum of the electric field obtained with the High Frequency Analyzer (HFA) of the Plasma Wave Experiment onboard Arase. (b) Electron density at the Arase location derived from the upper-hybrid resonance frequency, which was obtained from the HFA spectrum data. (c) Dynamic spectrum of the north-south component of the induction magnetometer data at SYO, Antarctica. (d) Echo power detected by the medium-frequency (MF) radar at SYO with an operating frequency of 2.4 MHz. (e) Eastward neutral wind velocity observed by the MF radar at SYO. Positive and negative values indicate eastward and westward, respectively. Black diamonds show the locations of polar mesosphere winter echoes, which were plotted when the echo power of the Program of the Antarctic Syowa Mesosphere, Stratosphere, and Troposphere/Incoherent Scatter Radar was greater than -10 dB at altitudes lower than 82 km.

detected at 63- to 82-km altitude with the PANSY radar at SYO and continued until 07:00 UT with temporal variations (Figure 4h). The energy of incident electrons that caused the echoes observed at 63 km was estimated to be ~ 500 keV by the calculation of the energy deposition rate using the MSIS-E-90 atmosphere model (Hedin, 1991; Jackman et al., 1980). Weak PMWE were also observed around 70 km at 03:00–04:00 UT during interval (A).

Corresponding mesospheric echoes were also detected with the medium-frequency (MF) radar with an operating frequency of 2.4 MHz at SYO. Figure 5 shows some supplementary data sets obtained by the Arase satellite and ground-based observation at SYO during 02:00–07:00 UT on 21 March. The echo power enhancement was observed with the MF radar at 55–70 km during 02:30–07:00 UT (Figure 5d), which are normally not observed during quiet conditions. Figure 5e shows the eastward neutral wind velocity observed by the MF radar at SYO. The black diamonds in this panel show the locations of PMWE, which were plotted when the echo power of the PANSY radar was greater than -10 dB at altitudes lower than 82 km. Large vertical shears in the horizontal wind velocity can be found at about 70 and 80 km, which substantially agree with the layered PMWE structure observed with the PANSY radar.

In the Northern Hemisphere, the quiet auroral arc was still stable on the high-latitude side of HUS, Iceland, just after the substorm onset (Figure 4d). The quiet arc was gradually replaced by an eastward propagating diffuse aurora that was elongated in the east-west direction, and the diffuse aurora expanded both equatorward and poleward after 04:30 UT (Movie S1 in the supporting information). Pulsating auroras appeared

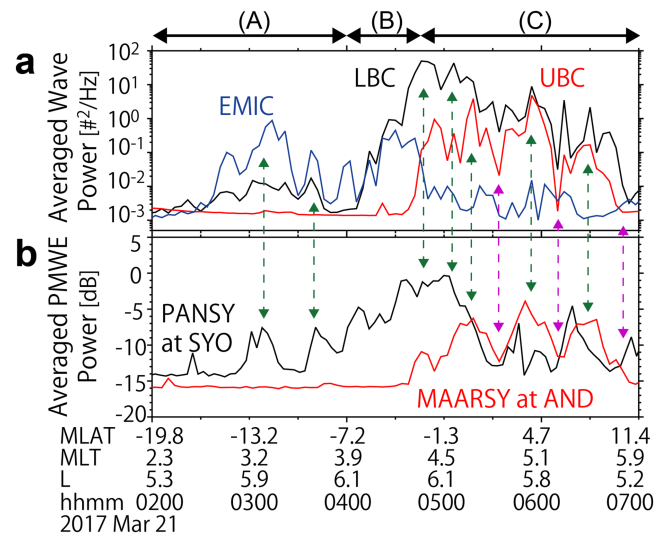


Figure 6. Comparison between magnetospheric plasma wave and PMWE powers. All data were averaged over 4 minutes to correspond to the sampling interval of the PANSY radar. (a) Power of the UCB (red), LBC (black), and EMIC (blue) waves averaged over corresponding frequencies ($0.5f_{ce}$ – $0.8f_{ce}$ for UCB, $0.1f_{ce}$ – $0.5f_{ce}$ for LBC, and 0.2 – 0.5 Hz for EMIC waves). The units of the averaged wave power are nT^2/Hz for the EMIC waves and pT^2/Hz for chorus waves, respectively. (b) PMWE powers observed with the PANSY radar (black) and MAARSY radar (red) averaged over mesospheric altitudes (60–78 km for PANSY and 55–75 km for MAARSY). PMWE = polar mesosphere winter echoes; EMIC = electromagnetic ion cyclotron; LBC = lower band chorus; UBC = upper band chorus; PANSY = Program of the Antarctic Syowa Mesosphere, Stratosphere, and Troposphere/Incoherent Scatter Radar; MAARSY = Middle Atmosphere Alomar Radar System.

from 04:45 UT until the end of the optical observation, corresponding to interval (C). Previous studies have found that pulsating auroras are caused by electrons with E of several tens of kiloelectron volts that are precipitated by interaction with LBC waves (S. Kasahara, Miyoshi, et al., 2018; Nishimura et al., 2010). After the auroral expansion, PMWE were observed at 57–75 km with the MAARSY radar at AND, Norway (Figure 4c). We believe that this is the first time PMWE have been observed in both hemispheres at exactly the same time. The PMWE observed at 57 km correspond to precipitation of relativistic electrons with $E \approx 1$ MeV.

We compare plasma wave and PMWE powers in Figure 6. All data plotted in this figure were averaged over 4 min to correspond to the sampling interval of the PANSY radar. The power of the UCB (red), LBC (black), and EMIC (blue) waves was averaged over corresponding frequencies, that is, $0.5f_{ce}$ – $0.8f_{ce}$ for upper band chorus, $0.1f_{ce}$ – $0.5f_{ce}$ for LBC, and 0.2 – 0.5 Hz for EMIC waves, where f_{ce} is the electron cyclotron frequency ($f_{ce} = eB/(2\pi m)$). The magnitude of local magnetic field observed by Arase was used for this calculation. The PMWE powers observed with the PANSY radar (black) and MAARSY radar (red) were averaged over 60–78 km for PANSY and 55–75 km for MAARSY. During interval (C), the PMWE powers in both hemispheres show trends quite similar to that of the chorus wave power. To illustrate this, matching maximum and minimum peaks are marked with green and purple arrows, respectively, in Figure 6. In addition, the PMWE observed at SYO during interval (A) appear to be related to the EMIC waves. During this interval, Pc 1 pulsations were also observed with the induction magnetometer at both SYO and HUS at frequencies of 0.2 – 0.5 Hz (see Figure 2 in Shiohawa et al., 2018, and Figure 5c), which is consistent with the dominant frequency of the EMIC waves observed by Arase.

3. Discussion

Our observational results are summarized as follows:

1. We observed the PMWE by the PANSY and MAARSY radars in the both hemispheres and EMIC waves and whistler mode chorus waves by Arase near the magnetic equator of the morningside magnetosphere at 03–07 UT on 21 March 2017, during the passage of the CIR.

2. During the expansion phase of the isolated substorm (interval [B]), during which Arase's footprints were located near SYO and HUS, the enhancement of PMWE was observed with the PANSY radar at SYO. The broadband plasma waves were simultaneously detected in the equatorial magnetosphere. CNA was also observed with the imaging riometer at SYO, which indicates the precipitation of energetic electrons with energies of several tens to several hundreds of kiloelectron volts.
3. During the recovery phase of the substorm (interval [C]), PMWE were observed with the PANSY and MAARSY radars in the both hemispheres and whistler mode chorus waves were detected in the magnetosphere. The temporal variations in the PMWE were similar to that of the chorus waves. Pulsating auroras appeared at HUS simultaneously with the chorus waves.
4. During the interval (A) before the substorm onset, PMWE and EMIC waves were simultaneously observed at SYO and Arase, respectively.
5. The MF radar at SYO detected the low-altitude echoes at 55–70 km intermittently during 02:30–07:00 UT, which are not usually observed during quiet condition and may be associated with the enhancement in the PMWE at SYO. The MF radar also detected large vertical shears in the horizontal wind velocity at about 70 and 80 km, which substantially agreed with the layered PMWE structure observed with the PANSY radar.

Item 1 indicates that the PMWE may be associated with the energetic electron precipitation during the passage of CIRs and HSS. It has been well known that the enhancement of radiation belt electrons occurs during CIRs and HSS (Baker & Li, 2003; Miyoshi et al., 2013; Miyoshi & Kataoka, 2005, 2008). Meredith et al. (2011) showed that the flux of both trapped and precipitating energetic electrons increases during HSS-driven geomagnetic storms, in particular, the precipitating $E > 30$ -keV electron flux peaks in 2100–1200 MLT at $4 < L < 7$ and in the prenoon sector at $7 < L < 9$. Kirkwood, Osepian, Belova, and Lee (2015) have reported that PMWE are closely related to the arrival of HSS, with PMWE appearing at heights as low as 56 km and persisting for up to 15 days after the HSS arrival. Similar PMWE enhancement after the arrival of CIRs and HSS was observed for the event analyzed in this study (Figure 2). This case study clarified that the process of plasma wave-particle interaction interposes between the arrival of CIRs and PMWE.

Regarding Item 5, the rough coincidence of the large wind shears with the PMWE layers implies that the PMWE were caused by the neutral turbulence due to the neutral wind shears. Since we do not have the measured values of neutral parameters and electron density needed to estimate the radar reflectivity, which are responsible for the temporal variation of the PMWE, we discuss the generation mechanism of the PMWE qualitatively only. The enhancement of the PMWE were probably triggered primarily by the energetic electron precipitation from the magnetosphere for the following reasons: (1) The PMWE were accompanied by CNA that is the indicator of the energetic electron precipitation just after the substorm onset (Item 2). (2) The PMWE showed the similar temporal variation to the magnetospheric plasma waves (Items 3 and 4). (3) The enhancement in the PMWE occurred in the both hemispheres (Item 3). It is interpreted that neutral turbulence layers had existed in the mesosphere due to the wind shears before the energetic electron precipitation; however, the echo power was not large enough to be detected because of low electron density. Then, the energetic electron precipitation caused the electron density enhancement in the mesosphere and finally the PMWE became detectable at the turbulence layers.

As for Item 2, our results are similar to those from recent PANSY radar observations. Nishiyama et al. (2018) have shown some good examples of PMWE and CNA simultaneously observed in the daytime during substorms. Kataoka et al. (2019) reported that the mesosphere echoes were observed at 65–70 km during the premidnight auroral breakup in association with CNA in the ionosphere and broadband noise in the magnetosphere. In this study, it was deduced from the PMWE observed at 63–8 km that the energetic electrons with E up to 500 keV were precipitated during the substorm expansion phase. Furthermore, the low-altitude echoes detected with the MF radar indicate the precipitation of more energetic electrons with E up to about 1 MeV (Item 5).

During the interval (B), a clear two-step geomagnetic variation was observed in the northward component at SYO and also at HUS and AND (not shown here). The first gradual negative variation that started around 04:00 UT is associated with the expansion phase onset of the substorm. The second rapid negative variation started around 04:23 UT at SYO and 04:26 UT both at HUS and AND and reached minimum around 04:43 UT at SYO, 04:46 UT at HUS, and 04:45 UT at AND (Figure 4i). Quiet auroral arc at HUS was located around

northern horizon during the first step, and the eastward and equatorward expansion of the diffuse aurora was observed during the second step. The rapid negative bay variation during the second step, corresponding to the intensification of the westward ionospheric current, can be explained by the enhancement in the ionospheric conductivity due to the auroral precipitation and/or the enhancement in the equatorward electric field. Since the negative bay variation was observed synchronously with the equatorward spread of the auroral precipitation region, the contribution of the conductivity enhancement should be significant. In addition, the observed eastward drift of the diffuse aurora is also consistent with the equatorward electric field. The eastward and equatorward expansion of the diffuse aurora suggests the development of magnetospheric convection. It is inferred that the development of the magnetospheric convection caused a shrinkage of the plasmasphere, which resulted in the exit of Arase from the plasmasphere around 04:45 UT. The similar magnetic variation between SYO, HUS, and AND during the second step implies that such an eastward and equatorward expansion of aurora region observed at HUS occurred almost simultaneously both at SYO and AND. On the other hand, PMWE during the interval (B) were enhanced only at SYO. This suggests that the energetic electrons were precipitated only in the Southern Hemisphere during the interval (B), and the precipitating electrons were originated from the inner magnetosphere well earthward from the inner edge of the plasma sheet (source region of the auroral particles), possibly, from the radiation belt. Such a north-south asymmetry of the energetic electron precipitation may be caused by the difference of the geomagnetic field intensity between SYO and AND (Torr et al., 1975). The magnitude of the magnetic field at 100-km altitude over SYO and AND calculated by the IGRF model is about 41,300 and 51,000 nT, respectively.

Item 3 strongly suggests that the chorus waves caused the REP (up to ~1 MeV) that leads to the PMWE. There had hardly been clear observational evidence that the chorus waves cause REP. Recently, Breneman et al. (2017) reported a case study where relativistic electron microbursts with energies from 220 keV to 1 MeV were observed simultaneously with whistler mode chorus waves near $L = 5.6$ and $MLT = 10.5$ during the recovery phase of a geomagnetic storm. Our results from simultaneous satellite and ground-based observations support that chorus waves can cause REP even for normal substorms that occurred during non-storm time period. It is remarkable that the PMWE occurred almost simultaneously both at SYO and AND during the interval (C), and furthermore, the temporal variation of the PMWE observed at AND was quite similar to that of the chorus waves, in spite of the large longitudinal separation from the Arase footprints. It is interpreted that chorus waves were generated through cyclotron resonance with anisotropic electrons between a few and tens of kiloelectron volts, which were injected from the nightside plasma sheet and drifted dawnward during the substorm (e.g., Miyoshi et al., 2013). The nonlinear growth of the chorus waves due to the energetic electrons was described by the theoretical and simulation study by Omura and Nunn (2011). Such a high correlation of VLF waves between SYO and AND has been reported by ground-based observations (Yamagishi, 1989). Yamagishi (1989) demonstrated by the numerical simulation that the simultaneous observation of the VLF wave packets between SYO and AND can be explained by the spread of the raypaths of the VLF waves as they travel from the magnetosphere to the ionosphere.

In order to examine whether the observed chorus waves can resonate with the relativistic electrons, we estimated the resonance energy (E_{res}) of electrons interacting with the observed LBC waves, according to Miyoshi, Oyama, et al. (2015). The relativistic Doppler-shifted cyclotron resonance condition is given by

$$\omega - k_{//}v_{//} = \frac{|\Omega_e|}{\gamma}, \quad (1)$$

where ω , $k_{//}$, $v_{//}$, Ω_e , and γ are the wave's angular frequency, parallel wave number, parallel speed of the electron, electron cyclotron angular frequency, and Lorentz factor ($\gamma = \left\{1 - (v_{//}^2 + v_{\perp}^2)/c^2\right\}^{-1/2}$), respectively (Omura & Nunn, 2011). Under the cold plasma approximation, the dispersion relation of the whistler mode waves that propagate along the field line is written by

$$k_{//} = \frac{\omega}{c} \sqrt{1 + \frac{\omega_{pe}}{\omega(|\Omega_e| - \omega)}}, \quad (2)$$

where ω_{pe} and c are the electron plasma frequency and the speed of light. By substituting (2) to (1), we estimated $v_{//}$ and subsequently E_{res} . Ω_e and ω_{pe} include the magnetic field intensity (B) and the

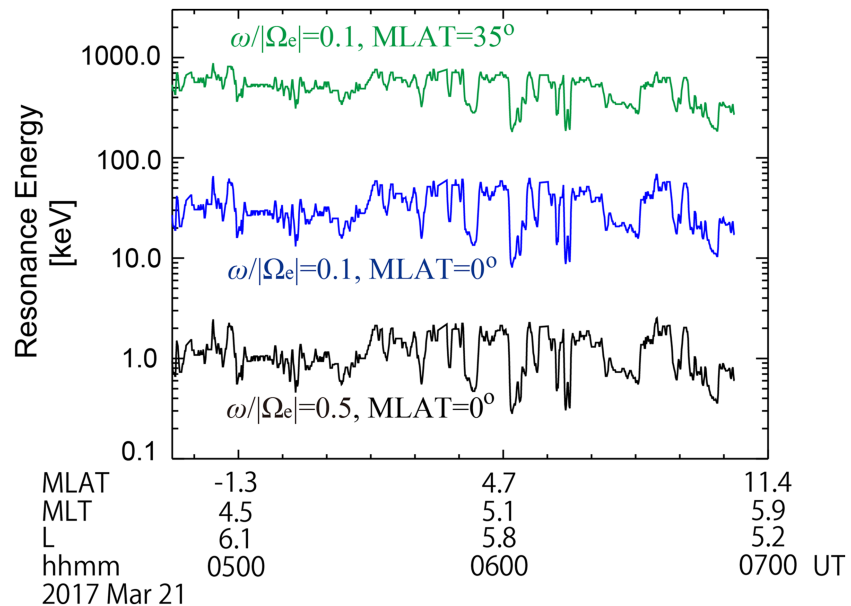


Figure 7. Electron resonance energy in the lower band chorus (LBC) waves observed by Arase at 04:45–0700 UT, which was calculated with equations (1) and (2). We assumed that the LBC waves were generated near the equatorial plane of the magnetosphere, and the LBC wave frequency (ω) was between $0.1 |\Omega_e|$ (blue curve) and $0.5 |\Omega_e|$ (black curve). The resonance energy calculated assuming that the LBC waves with $f = 0.1 |\Omega_e|$ propagated to higher latitudes and resonated with electrons at a magnetic latitude of 35° was added to the figure (green curve).

electron density (N_e), respectively. B was obtained by using the Tsyganenko and Sitnov TS04 model, and N_e was derived from the upper-hybrid resonance (UHR) frequency, which was obtained by the High Frequency Analyzer of the Plasma Wave Experiment onboard Arase (Figures 5a and 5b; Kumamoto et al., 2018). The typical values of N_e outside the plasmasphere were from a few to 20 cm^{-3} , and N_e was assumed to be constant along the field line (e.g., Miyoshi, Oyama, et al., 2015). Figure 7 shows E_{res} estimated assuming that the resonance occurred at the magnetic equator and the angular frequency of the LBC wave is between $0.1 |\Omega_e|$ and $0.5 |\Omega_e|$. The estimated maximum values of E_{res} (at $\omega = 0.1 |\Omega_e|$) were about 10–100 keV at 04:45–07:00 UT (blue line). This can account for simultaneous detection on the pulsating auroras and CNA. In fact, it has been reported that CNA absorption is overlapped with the pulsating aurora (e.g., Grandin et al., 2017). However, E_{res} was too low to cause the low-altitude PMWE. If LBC waves propagate to higher latitudes and resonate with energetic electrons there, E_{res} increases with increasing magnetic field intensity (Miyoshi et al., 2010; Miyoshi, Oyama, et al., 2015). We found that E_{res} became close to 1 MeV if the resonance occurred at a magnetic latitude of 35° (green line)

As for Item 4, the PMWE observed at SYO during interval (A) can be related to electron precipitation due to wave-particle interaction with EMIC waves because there is no other candidate. Before 04:45 UT, Arase was inside the plasmasphere (the plasmapause position is shown by a vertical thick arrow at the top of Figure 5), in which the UHR frequency was around 100 kHz and N_e at Arase's location was estimated to be between 50 and 150 cm^{-3} from the UHR frequency. Our interpretation is that EMIC waves were generated inside the plasmasphere by ring current ions ($E \sim 1\text{--}300 \text{ keV}$) with temperature anisotropy. This anisotropy was caused by magnetospheric compression due to increasing solar wind dynamic pressure during 01:00–06:00 UT (Figure 3d; Olson & Lee, 1983). Such EMIC waves propagate along the field lines and are often observed as Pc 1 pulsations on the ground. The EMIC waves and the Pc 1 pulsations shown in this paper have already been analyzed by Shiokawa et al. (2018). They showed that the Pc 1 pulsations with a similar dominant frequency were observed at subauroral latitudes over a wide local time range from midnight to afternoon sectors (cf. Figure 4b). They also analyzed the high-energy (1.0–1.2 MeV) electron fluxes in the radiation belts measured by the extremely high energy electron experiments (Higashio et al., 2018) onboard Arase and found the loss of radiation belt electrons at $L > 5.3$, which is consistent with the occurrence of PMWE in this study. Kurita et al. (2018) also focused on the data obtained at 07:00–08:40 UT on the same day by the Arase, Van Allen Probes, and ground-based network observations and clearly demonstrated

Acknowledgments

Mark Kurban, M. Sc., from Edanz Group (www.edanzediting.com/ac) edited a draft of this manuscript. This study was supported by the Japan Society for the Promotion of Science (JSPS), Grants-in-Aid for Scientific Research (S) 15H05747, (A) 25247075, (A) 15H02628, and (B) 24340121 and Specially Promoted Research Grant 16H06286 and Scientific Research on Innovative Areas Grant 15H05815 of the Japan Ministry of Education, Culture, Sports, and Technology (MEXT). This study was also supported by projects KP-2, KP-5, and KP-301 of the National Institute of Polar Research (NIPR), and JST CREST Grant Number JPMJCR1663, Japan. PANSY is a multi-institutional project with a core comprising the University of Tokyo and NIPR. The observations at Syowa Station were mainly supported by the Research Program of Japanese Antarctic Research Expedition (JARE) of the MEXT. The database construction for the ground-based instruments was partly supported by the Interuniversity Upper atmosphere Global Observation NETWORK (IUGONET) project (<http://www.iugonet.org/>). The production of this paper was supported by a subsidy from the NIPR. Science data from the ERG (Arase satellite) were obtained from the ERG Science Center operated by ISAS/JAXA and ISEE/Nagoya University (https://ergsc.isee.nagoya-u.ac.jp/data_info/index.shtml.en). The MGF v02.01, PWE/OFA v02.01, PWE/HFA v01.01, and ERG Orbit L2 v02 were analyzed in this study. The MAARSY radar data are available at the IAP FTP site (ftp://ftp.iap-kborn.de/data-in-publications/Tanaka_JGR2019/). The PANSY radar observation data are available at the project website (<http://pansy.eps.s.u-tokyo.ac.jp/en/data/>). PANSY high-resolution data used in this study are described in Sato et al. (2014) and available by request. Contact Kaoru Sato (kaoru@eps.s.u-tokyo.ac.jp). The data obtained with the fluxgate magnetometer, induction magnetometer, imaging riometer, and MF radar at Syowa Station are available at the NIPR IUGONET website (<http://iugonet0.nipr.ac.jp/data/>). The solar wind data and AE index were downloaded from the NASA's Space Physics Data Facility (https://spdf.gsfc.nasa.gov/pub/data/omni/omni_cdaweb/). The AE index was originally provided by the World Data Center for Geomagnetism, Kyoto University. These data can be downloaded and analyzed using the software SPEDAS (<http://spedas.org>) with the plugins IUGONET and ERG.

that the loss of megaelectron volt electron fluxes were induced by EMIC waves. It should be noted that there is a possibility that Arase's footprints were far from SYO during the interval (A). Even in such a case, we speculate that the PMWE may be related to REP caused by the EMIC waves because the Pc 1 pulsations were observed over a wide range of longitude (Shiokawa et al., 2018).

During interval (A), no PMWE was detected by the MAARSY radar at AND (Figure 4c). There are two possibilities for the absence of PMWE at AND. One is because the precipitation occurred in the nighttime before the sunrise at AND. The PMWE are not usually observed in the nighttime because of low electron density in the mesosphere (Kirkwood, 2007; Nishiyama et al., 2015). The sunrise time at AND is 03:22 UT at 70 km and 03:30 UT at 60 km, whereas the sunrise time at SYO is 01:58 UT at 70 km and 02:05 UT at 60 km. Thus, it is deduced that the background electron density in the mesosphere at AND was not enough to reflect the backscatter echoes even when the energetic electrons were precipitated by the EMIC waves at 03:00–04:00 UT. On the other hand, the background electron density in the sunlit mesosphere at SYO was high enough to make the PMWE detectable. The other possibility may be the absence of atmospheric turbulence with spatial scales of the radar half wavelength (~ 3 m) in the mesosphere at AND, as stated above. Such temporal variation in the turbulence causes the nonperfect correlation between the PMWE and plasma waves in Figure 6.

Our unique and comprehensive observational data sets are consistent with the following plausible scenario. First, neutral turbulence layers were formed in the mesosphere by wind shear. The arrival of CIR in front of HSS caused magnetospheric compression, followed by the generation of EMIC waves in the inner magnetosphere (Figure 4b(1)). The EMIC waves resonated with and precipitated energetic electrons and caused the enhancement of the electron density in the mesosphere, resulting in PMWE at 03:00–04:00 UT. An isolated substorm occurred at 04:00 UT during CIR passage, and energetic electrons were injected from the nightside plasma sheet and drifted downward to generate the chorus waves (Figure 4b(2)). The chorus waves precipitated energetic electrons including sub-megaelectron volt and megaelectron volt electrons into the polar atmosphere by cyclotron resonance scattering, with propagation to higher latitudes along and across the field lines. The energetic electron precipitation caused pulsating auroras in the *E* region ionosphere, CNA in the *D* region ionosphere, and PMWE in the mesosphere.

4. Conclusions

We compared between the plasma waves and PMWE observed simultaneously by Arase and high-power atmosphere radars, the PANSY and MAARSY, on the ground in both hemispheres under the ideal condition during the passage of CIR. The results showed an evidence that the whistler mode chorus waves as well as the EMIC waves in the magnetosphere can drive the precipitation of energetic electrons, including relativistic electrons, which makes the PMWE detectable at 55–80 km in both Northern and Southern Hemispheres, even during non-storm time substorm. Since chorus waves occur commonly in the morningside magnetosphere during substorms, the impact on the atmosphere is significant. Therefore, it is necessary to investigate the chorus-driven REP statistically in future.

We also suggested that various phenomena observed in near-Earth space, such as magnetospheric plasma waves (EMIC waves and chorus waves), pulsating auroras, CNA, and PMWE, can be consistently explained by the interaction between the high-speed solar wind containing CIRs and the magnetosphere. CIRs are main sources of geomagnetic disturbances during the declining phase of the solar cycle and solar minimum (Kataoka & Miyoshi, 2006; Miyoshi & Kataoka, 2005; Richardson et al., 2006; Tsurutani et al., 1995); therefore, this event is not rare but rather a common atmospheric response caused by interaction between recurrent large-scale solar wind structures and near-Earth space.

References

- Baker, D. N., & Li, X. (2003). Relativistic electron flux enhancements during strong geomagnetic activity. *Disturbances in Geospace: The Storm-Substorm Relationship*, *Geophysical Monograph*, 142. <https://doi.org/10.1029/142GM18>
- Balsley, B. B., Ecklund, W. L., & Fritts, D. C. (1983). VHF echoes from the high-latitude mesosphere and lower thermosphere: Observations and interpretations. *Journal of the Atmospheric Sciences*, 40(10), 2451–2466.
- Belova, E., Kirkwood, S., Ekeberg, J., Osepian, A., Haggstrom, I., Nilsson, H., & Rietveld, M. (2005). The dynamical background of polar mesosphere winter echoes from simultaneous EISCAT and ESRAD observations. *Annales Geophysicae*, 23, 1239–1247. <https://doi.org/10.5194/angeo-23-1239-2005>

- Belova, E., Smirnova, M., Rietveld, M. T., Isham, B., Kirkwood, S., & Siergienko, T. (2008). First observation of the overshoot effect for polar mesospheric winter echoes during radiowave electron temperature modulation. *Geophysical Research Letters*, *35*, L03110. <https://doi.org/10.1029/2007GL032457>
- Breneman, A. W., Crew, A., Sample, J., Klumpar, D., Johnson, A., Agapitov, O., et al. (2017). Observations directly linking relativistic electron microbursts to whistlermode chorus: Van Allen Probes and FIREBIRD II. *Geophysical Research Letters*, *44*, 11,265–11,272. <https://doi.org/10.1002/2017GL075001>
- Crooker, N. U., & Cliver, E. W. (1994). Postmodern view of M-regions. *Journal of Geophysical Research*, *99*(A12), 23,383–23,390. <https://doi.org/10.1029/94JA02093>
- Czechowsky, P., Reid, I. M., Rüster, R., & Schmidt, G. (1989). VHF radar echoes observed in the summer and winter polar mesosphere over Andoya, Norway. *Journal of Geophysical Research*, *94*(D4), 5199–5217. <https://doi.org/10.1029/JD094iD04p05199>
- Grandin, M., Kero, A., Partamies, N., McKay, D., Whiter, D., Kozlovsky, A., & Miyoshi, Y. (2017). Observation of pulsating aurora signatures in cosmic noise absorption data. *Geophysical Research Letters*, *44*, 5292–5300. <https://doi.org/10.1002/2017GL073901>
- Hedin, A. E. (1991). Extension of the MSIS thermospheric model into the middle and lower atmosphere. *Journal of Geophysical Research*, *96*, 1159–1172. <https://doi.org/10.1029/90JA02125>
- Hendry, A. T., Rodger, C. J., & Clilverd, M. A. (2017). Evidence of sub-MeV EMIC-driven electron precipitation. *Geophysical Research Letters*, *44*, 1210–1218. <https://doi.org/10.1002/2016GL071807>
- Higashio, N., Takashima, T., Shinohara, I., & Matsumoto, H. (2018). The extremely high-energy electron experiments (XEP) onboard the Arase satellite. *Earth, Planets and Space*, *70*(1). <https://doi.org/10.1186/s40623-018-0901-x>
- Jackman, C. H., Frederick, J. E., & Stolarski, R. S. (1980). Production of odd nitrogen in the stratosphere and mesosphere: An intercomparison of source strengths. *Journal of Geophysical Research*, *85*, 7495–7505. <https://doi.org/10.1029/JC085iC12p07495>
- Kasahara, S., Miyoshi, Y., Yokota, S., Mitani, T., Kasahara, Y., Matsuda, S., et al. (2018). Pulsating aurora from electron scattering by chorus waves. *Nature*, *554*, 337–340. <https://doi.org/10.1038/nature25505>
- Kasahara, Y., Kasaba, Y., Kojima, H., Yagitani, S., Ishisaka, K., Kumamoto, A., et al. (2018). The Plasma Wave Experiment (PWE) on board the Arase (ERG) satellite. *Earth, Planets and Space*, *70*, 86. <https://doi.org/10.1186/s40623-018-0842-4>
- Kataoka, R., & Miyoshi, Y. (2006). Flux enhancement of radiation belt electrons during geomagnetic storms driven by coronal mass ejections and corotating interaction regions. *Space Weather*, *4*, S09004. <https://doi.org/10.1029/2005SW000211>
- Kataoka, R., Nishiyama, T., Tanaka, Y.-M., Kadokura, A., Uchida, H. A., Ebihara, Y., et al. (2019). Transient ionization of the mesosphere during auroral breakup: Arase satellite and ground-based conjugate observations at Syowa Station. *Earth, Planets and Space*, *71*, 9. <https://doi.org/10.1186/s40623-019-0989-7>
- Kirkwood, S. (2007). Polar mesosphere winter echoes: A review of recent results. *Advances in Space Research*, *40*, 751–757. <https://doi.org/10.1016/j.asr.2007.01.024>
- Kirkwood, S., Barabash, V., Belova, E., Nilsson, H., Rao, T. N., Stebel, K., et al. (2002). Polar mesosphere winter echoes during solar proton events. *Advances in Polar Upper Atmosphere Research*, *16*, 111–125.
- Kirkwood, S., Chilson, P., Belova, E., Dalin, P., Häggström, I., Rietveld, M., & Singer, W. (2006). Infrasound—The cause of polar mesosphere winter echoes? *Annales Geophysicae*, *24*, 475–491. <https://doi.org/10.5194/angeo-24-475-2006>
- Kirkwood, S., Osepian, A., Belova, E., & Lee, Y.-S. (2015). High-speed solar wind streams and polar mesosphere winter echoes at Troll, Antarctica. *Annales Geophysicae*, *33*, 609–622. <https://doi.org/10.5194/angeo-33-609-2015>
- Kirkwood, S., Osepian, A., Belova, E., Urban, J., Pérot, K., & Sinha, A. K. (2015). Ionization and NO production in the polar mesosphere during high-speed solar wind streams: Model validation and comparison with NO enhancements observed by Odin-SMR. *Annales Geophysicae*, *33*, 561–572. <https://doi.org/10.5194/angeo-33-561-2015>
- Kumamoto, A., Tsuchiya, F., Kasahara, Y., Kasaba, Y., Kojima, H., Yagitani, S., et al. (2018). High Frequency Analyzer (HFA) of Plasma Wave Experiment (PWE) onboard the Arase spacecraft. *Earth Planets Space*, *70*, 82. <https://doi.org/10.1186/s40623-018-0854-0>
- Kurita, S., Miyoshi, Y., Shiokawa, K., Higashio, N., Mitani, T., Takashima, T., et al. (2018). Rapid loss of relativistic electrons by EMIC waves in the outer radiation belt observed by Arase, Van Allen Probes, and the PWING ground stations. *Geophysical Research Letters*, *45*, 12,720–12,729. <https://doi.org/10.1029/2018GL080262>
- La Hoz, C., & Havnes, O. (2008). Artificial modification of polar mesospheric winter echoes with an RF heater: Do charged dust particles play an active role? *Journal of Geophysical Research*, *113*, D19205. <https://doi.org/10.1029/2008JD010460>
- Lattek, R., Singer, W., Rapp, M., Vandeppeer, B., Renkowitz, T., Zecha, M., & Stober, G. (2012). MAARSY—The new MST radar on Andoya-system description and first results. *Radio Science*, *47*, RS006. <https://doi.org/10.1029/2011RS004775>
- Lattek, R., & Strelnikova, I. (2015). Extended observations of polar mesosphere winter echoes over Andøya (69°N) using MAARSY. *Journal of Geophysical Research: Atmospheres*, *120*, 8216–8226. <https://doi.org/10.1002/2015JD023291>
- Lübken, F.-J., Strelnikov, B., Rapp, M., Singer, W., Lattek, R., Brattli, A., et al. (2006). The thermal and dynamical state of the atmosphere during polar mesosphere winter echoes. *Atmospheric Chemistry and Physics*, *6*, 13–24. <https://doi.org/10.5194/acp-6-13-2006>
- Lyons, L. R., & Thorne, R. M. (1972). Parasitic pitch angle diffusion of radiation belt particles by ions cyclotron waves. *Journal of Geophysical Research*, *77*, 5608–5617. <https://doi.org/10.1029/JA077i028p05608>
- Matsuda, S., Kasahara, Y., Kojima, H., Kasaba, Y., Yagitani, S., Ozaki, M., et al. (2018). Onboard software of plasma wave experiment aboard Arase: Instrument management and signal processing of waveform capture/onboard frequency analyzer. *Earth, Planets and Space*, *70*, 75. <https://doi.org/10.1186/s40623-018-0838-0>
- Matsuoka, A., Teramoto, M., Nomura, R., Nose, M., Fujimoto, A., Tanaka, Y., et al. (2018). The ARASE (ERG) magnetic field investigation. *Earth, Planets and Space*, *70*, 43. <https://doi.org/10.1186/s40623-018-0800-1>
- Meredith, N. P., Horne, R. B., Lam, M. M., Denton, M. H., Borovsky, J. E., & Green, J. C. (2011). Energetic electron precipitation during high-speed solar wind stream driven storms. *Journal of Geophysical Research*, *116*, A05223. <https://doi.org/10.1029/2010JA016293>
- Miyoshi, Y., & Kataoka, R. (2005). Ring current ions and radiation belt electrons during geomagnetic storms driven by coronal mass ejections and corotating interaction regions. *Geophysical Research Letters*, *32*, L21105. <https://doi.org/10.1029/2005GL024590>
- Miyoshi, Y., & Kataoka, R. (2008). Flux enhancement of the outer radiation belt electrons after the arrival of stream interaction regions. *Journal of Geophysical Research*, *113*, A03S09. <https://doi.org/10.1029/2007JA0125>
- Miyoshi, Y., Kataoka, R., Kasahara, Y., Kumamoto, A., Nagai, T., & Thomsen, M. (2013). High-speed solar wind with southward interplanetary magnetic field causes relativistic electron flux enhancement of the outer radiation belt via enhanced condition of whistler waves. *Geophysical Research Letters*, *40*, 4520–4525. <https://doi.org/10.1002/grl.50916>

- Miyoshi, Y., Katoh, Y., Nishiyama, T., Sakanoi, T., Asamura, K., & Hirahara, M. (2010). Time of flight analysis of pulsating aurora electrons, considering wave-particle interactions with propagating whistler mode waves. *Journal of Geophysical Research*, *115*, A10312. <https://doi.org/10.1029/2009JA015127>
- Miyoshi, Y., Oyama, S., Saito, S., Kurita, S., Fujiwara, H., Kataoka, R., et al. (2015). Energetic electron precipitation associated with pulsating aurora: EISCAT and Van Allen Probe observations. *Journal of Geophysical Research: Space Physics*, *120*, 2754–2766. <https://doi.org/10.1002/2014JA020690>
- Miyoshi, Y., Saito, S., Seki, K., Nishiyama, T., Kataoka, R., Asamura, K., et al. (2015). Relation between fine structure of energy spectra for pulsating aurora electrons and frequency spectra of whistler mode chorus waves. *Journal of Geophysical Research: Space Physics*, *120*, 7728–7736. <https://doi.org/10.1002/2015JA021562>
- Miyoshi, Y., Sakaguchi, K., Shiokawa, K., Evans, D., Albert, J., Connors, M., & Jordanova, V. (2008). Precipitation of radiation belt electrons by EMIC waves, observed from ground and space. *Geophysical Research Letters*, *35*, L23101. <https://doi.org/10.1029/2008GL035727>
- Miyoshi, Y., Shinohara, I., Takashima, T., Asamura, K., Higashio, N., Mitani, T., et al. (2018). Geospace exploration project ERG. *Earth Planets Space*, *70*(101). <https://doi.org/10.1186/s40623-018-0862-0>
- Nishimura, Y., Bortnik, J., Li, W., Thorne, R. M., Lyons, L. R., Angelopoulos, V., et al. (2010). Identifying the driver of pulsating aurora. *Science*, *330*, 81–84. <https://doi.org/10.1126/science.1193186>
- Nishiyama, T., Sato, K., Nakamura, T., Tsutsumi, M., Sato, T., Kohma, M., et al. (2015). Height and time characteristics of seasonal and diurnal variations in PMWE based on 1 year observations by the PANSY radar (69.0°S, 39.6°E). *Geophysical Research Letters*, *42*, 2100–2108. <https://doi.org/10.1002/2015GL063349>
- Nishiyama, T., Sato, K., Nakamura, T., Tsutsumi, M., Sato, T., Tanaka, Y.-M., et al. (2018). Simultaneous observations of polar mesosphere winter echoes and cosmic noise absorptions in a common volume by the PANSY radar (69.0°S, 39.6°E). *Journal of Geophysical Research: Space Physics*, *123*(6), 5019–5032. <https://doi.org/10.1029/2017JA024717>
- Olson, J. V., & Lee, L. C. (1983). Pc1 wave generation by sudden impulses. *Planetary and Space Science*, *31*, 295–302. [https://doi.org/10.1016/0032-0633\(83\)90079-X](https://doi.org/10.1016/0032-0633(83)90079-X)
- Omura, Y., & Nunn, D. (2011). Triggering process of whistler mode chorus emissions in the magnetosphere. *Journal of Geophysical Research*, *116*, A05205. <https://doi.org/10.1029/2010JA016280>
- Ozaki, M., Shiokawa, K., Miyoshi, Y., Hosokawa, K., Oyama, S., Yagitani, S., et al. (2018). Microscopic observations of pulsating aurora associated with chorus element structures: Coordinated Arase satellite-PWING observations. *Geophysical Research Letters*, *45*, 12,125–12,134. <https://doi.org/10.1029/2018GL079812>
- Ozaki, M., Shiokawa, K., Miyoshi, Y., Kataoka, R., Connors, M., Inoue, T., et al. (2018). Discovery of 1 Hz range modulation of isolated proton aurora at subauroral latitudes. *Geophysical Research Letters*, *45*, 1209–1217. <https://doi.org/10.1002/2017GL076486>
- Ozaki, M., Shiokawa, K., Miyoshi, Y., Kataoka, R., Yagitani, S., Inoue, T., et al. (2016). Fast modulations of pulsating proton aurora related to subpacket structures of Pc1 geomagnetic pulsations at subauroral latitudes. *Geophysical Research Letters*, *43*, 7859–7866. <https://doi.org/10.1002/2016GL070008>
- Ozaki, M., Yagitani, S., Kasahara, Y., Kojima, H., Kasaba, Y., Kumamoto, A., et al. (2018). Magnetic search coil (MSC) of Plasma Wave Experiment (PWE) aboard the Arase (ERG) satellite. *Earth, Planets and Space*, *70*, 76. <https://doi.org/10.1186/s40623-018-0837-1>
- Rapp, M., & Lübken, F.-J. (2004). Polar mesosphere summer echoes (PMSE): Review of observations and current understanding. *Atmospheric Chemistry and Physics*, *4*, 2601–2633. <https://doi.org/10.5194/acp-4-2601-2004>
- Richardson, I. G., Webb, D. F., Zhang, J., Berdichevsky, D. B., Biesecker, D. A., Kasper, J. C., et al. (2006). Major geomagnetic storms (Dst ≤ −100 nT) generated by corotating interaction regions. *Journal of Geophysical Research*, *111*, A07S09. <https://doi.org/10.1029/2005JA011476>
- Saito, T. (1969). Geomagnetic pulsations. *Space Science Reviews*, *10*(3), 319–412. <https://doi.org/10.1007/BF00203620>
- Sato, K., Tsutsumi, M., Sato, T., Nakamura, T., Saito, A., Tomikawa, Y., et al. (2014). Program of the Antarctic Syowa MST/IS radar (PANSY). *Journal of Atmospheric and Solar-Terrestrial Physics*, *118*, 2–15. <https://doi.org/10.1016/j.jastp.2013.08.022>
- Shinnhuber, M., Nieder, H., & Wieters, N. (2012). Energetic particle precipitation and the chemistry of the mesosphere/lower thermosphere. *Surveys in Geophysics*, *33*, 1281–1334. <https://doi.org/10.1007/s10712-012-9201-3>
- Shiokawa, K., Ozaki, M., Kadokura, A., Endo, Y., Sakanoi, T., Kurita, S., et al. (2018). Purple auroral rays and global Pc1 pulsations observed at the CIR-associated solar wind density enhancement on March 21. *Geophysical Research Letters*, *45*(20), 10,819–10,828. <https://doi.org/10.1029/2018GL079103>
- Tanaka, Y.-M., Ishii, M., Murayama, Y., Kubota, M., Mori, H., Yamamoto, M.-Y., et al. (2005). Comparison between CNA and energetic electron precipitation: Simultaneous observation by Poker Flat Imaging Riometer and NOAA satellite. *Annales Geophysicae*, *23*, 1555–1563. <https://doi.org/10.5194/angeo-23-1555-2005>
- Thorne, R. M. (1977). Energetic radiation belt electron precipitation: A natural depletion mechanism for stratospheric ozone. *Science*, *195*, 287–289. <https://doi.org/10.1126/science.195.4275.287>
- Thorne, R. M., & Kennel, C. F. (1971). Relativistic electron precipitation during magnetic storm phase. *Journal of Geophysical Research*, *76*, 4446–4453. <https://doi.org/10.1029/JA076i019p04446>
- Torr, D. G., Torr, M. R., Walker, J. C. G., & Hoffman, R. A. (1975). Particle precipitation in the South Atlantic geomagnetic anomaly. *Planetary and Space Science*, *23*(1), 15–26. [https://doi.org/10.1016/0032-0633\(75\)90064-1](https://doi.org/10.1016/0032-0633(75)90064-1)
- Tsurutani, B. T., Gonzalez, W. D., Gonzalez, A. L. C., Tang, F., Arballo, J. K., & Okada, M. (1995). Interplanetary origin of geomagnetic activity in the declining phase of the solar cycle. *Journal of Geophysical Research*, *100*(A11), 21,717–21,733. <https://doi.org/10.1029/95JA01476>
- Tsyganenko, N. A., & Sitnov, M. I. (2005). Modeling the dynamics of the inner magnetosphere during strong geomagnetic storms. *Journal of Geophysical Research*, *110*, A03208. <https://doi.org/10.1029/2004JA010798>
- Turunen, E., Kero, A., Verronen, P. T., Miyoshi, Y., Oyama, S.-I., & Saito, S. (2016). Mesospheric ozone destruction by high-energy electron precipitation associated with pulsating aurora. *Journal of Geophysical Research: Atmospheres*, *121*, 11,852–11,861. <https://doi.org/10.1002/2016JD025015>
- Yamagishi, H. (1989). ELF emission in high latitudes—Ray path calculation and ground-satellite observations. *Memoirs of National Institute of Polar Research Ser. A*, *19*, 1–120. <http://id.nii.ac.jp/1291/00003511/>